Multi-cell Active Acoustic Metamaterial with Programmable Bulk Modulus

Wael Akl and Amr Baz

Journal of Intelligent Material Systems and Structures 2010; 21; 541 originally published online Jan 12, 2010;
DOI: 10.1177/1045389X09359434

Multi-cell Active Acoustic Metamaterial with Programmable Bulk Modulus

WAEL AKL[1] AND AMR BAZ[2,*]

[1]*Design and Production Engineering Department, Ain Shams University, Cairo, Egypt*

[2]*Mechanical Engineering Department, University of Maryland, College Park, MD, USA*

ABSTRACT: Considerable interest has been devoted to the development of various classes of acoustic metamaterials that can control the propagation of acoustical wave energy through these materials. However, all the currently exerted efforts are focused on studying passive metamaterials with fixed material properties. In this article, the emphasis is placed on the development of a new class of composite acoustic metamaterials with effective bulk moduli that are programmed to vary according to any prescribed pattern along the volume of the metamaterial. The composite consists of an acoustic cavity, which is coupled with an array of actively controlled Helmholtz resonator to enable the control of the effective bulk modulus distribution along the cavity. The theoretical analysis of this class of multi-cell *c*omposite *a*ctive *a*coustic *m*eta*m*aterials (CAAMM) is presented and the theoretical predictions are determined when the Helmholtz resonators are provided with piezoelectric boundaries. These smart boundaries are used to control the overall bulk modulus of the cavity/resonator assembly through direct acoustic pressure feedback. The interaction between the neighboring cells of the composite metamaterial is modeled using a lumped-parameter approach. Numerical examples are presented to demonstrate the performance characteristics of the proposed CAAMM and its potential for generating prescribed spatial and spectral patterns of bulk modulus variation.

Key Words: active acoustic metamaterials, effective bulk modulus, multi-cell composite metamaterials, Helmholtz resonators with piezoelectric boundaries.

NOMENCLATURE

A	Cross-sectional area of cavity
A_H	Cross-sectional area of Helmholtz resonator cavity
a	Cross-sectional area of Helmholtz resonator neck
B_e	Effective bulk modulus of the acoustic cavity
B_f	Bulk modulus of the fluid in the cavity
B_r	Relative bulk modulus of the acoustic cavity
C_F	Acoustic compliance of the acoustic cavity
C_D	Open-loop compliance of the piezo-diaphragm
C_{DC}	Closed-loop compliance of piezo-diaphragm
C_H	Acoustic compliance of the Helmholtz resonator
C_P	Capacitance connected in series with the piezo-diaphragm
c_f	Speed of sound sonic in the fluid domain
c_p	Speed of sound in the piezoelectric diaphragm
D	Electrical displacement
d_A	Effective piezoelectric coefficient
E	Electrical field
G	Feedback gain
K_D	Stiffness of the flexible diaphragm
K_{DC}	Closed-loop stiffness of the piezoelectric diaphragm
L_D	Dynamic mass of diaphragm
L_F	Electric-acoustical inductance of cavity
L_P	Inductor connected in parallel with piezoelectric diaphragm
l	Length of Helmholtz resonator neck
l_H	Length of Helmholtz resonator cavity
l_p	Thickness of flexible diaphragm in the Helmholtz resonator
p	Fluid pressure in the time domain
P	Fluid pressure in the Laplace domain
Δp	Pressure drop along cavity
Δp_P	Pressure across piezo-diaphragm
Q	Volumetric flow rate
q	Electrical charge
S	Strain
s^E	Piezoelectric compliance
s	Laplace complex number
T	Mechanical stress
V_P	Piezoelectric voltage

*Author to whom correspondence should be addressed. E-mail: baz@umd.edu
Figures 3, 9–13 and 17–22 appear in color online: http://jim.sagepub.com

1045-389X/10/05 0541–16 $10.00/0 DOI: 10.1177/1045389X09359434

Greek Symbols

- ε Permittivity
- ρ_f Density of the fluid inside the cavity
- ρ_D Density of the flexible diaphragm
- ϕ Electrical to acoustic domain transformer turn ratio
- ω Frequency

Subscripts

- f Fluid domain
- e Effective
- p Piezoelectric
- D Flexible diaphragm
- CD Closed loop
- H Helmholtz part specific

INTRODUCTION

EXTENSIVE research is currently focusing on the modeling and development of metamaterials with specific optical, electromagnetic, and acoustical properties, which are unachievable using natural materials. All these efforts aim at controlling the behavior of various wave types (electromagnetic and acoustic) to achieve perfect wave cloaking, improved ultrasonic imaging, or perfect lenses (Lapine, 2007; Shamonina and Solymar, 2007; Gil et al., 2008).

All the attempts to control the wave propagation behavior are focused on effectively managing the density ρ and/or the bulk modulus B of the medium. Two different approaches exist for synthesizing materials with bulk's moduli that are not available in nature. The first approach focuses on combining two different isotropic materials in a composite form to yield anisotropic properties that can influence the spatial wave propagation patterns. Examples of this approach include the attempts to produce single or double negative acoustic metamaterials whereby either ρ, B, or both assume negative values (Jensen and Chan, 2004; Mei et al., 2006; Chan et al., 2006; Ding et al., 2007; Huang et al., 2009). In the second approach, acoustic impedance mismatch is introduced along the path of wave propagation by integrating flexible sections into the rigid-walled ducts in order to vary the speed of sound and effective bulk modulus at these sections (Choi and Kim, 2002; Chiu et al., 2006).

Due to the coupling nature of the density and the bulk modulus, which directly affect the speed of sound in any continuous domain, various attempts to develop composite materials with homogenized properties always had an impact on both the density and the bulk modulus simultaneously. Attempts to introduce, for example the perfect lens (Pendry, 2000; Shen and Platzman, 2002; Merlin 2004) were focused on modeling the behavior of optical waves passing through a parallel-sided slab of material with negative refractive index. This has shown to produce remarkable results, due to double focusing effect (when properly selecting the slab dimensions) and the impedance match with the surrounding environment resulting in no reflections at the boundaries. Refractive index in optical or electromagnetic waves is analogous to the speed of sound in acoustics. Cummer and Shurig (2007) and Cummer et al. (2008a,b), have used this analogy between the electromagnetic and acoustic waves to theoretically design a material with specific density and bulk modulus distribution in order to realize an acoustic cloak. Sonic crystals, for example, which are composed of solid sound scatterers arranged in specific patterns and immersed in a fluid domain are an example of a composite material that has fixed effective density and bulk modulus (Torrent et al., 2006; Torrent and Sanchez-Dehesa, 2007, 2008). In their scope of investigation, the sonic crystals used, behave as effective homogeneous acoustic metamaterials whose parameters (bulk modulus B and dynamical mass density ρ) are mainly determined by the fraction of volume occupied by the scatterers and their refractive properties (Cervera et al., 2001; Krokhin et al., 2003; Torrent et al., 2007). However, the obtained effective parameters are highly dependent on the acoustic frequency range, and can be tailored for small frequency band based on the passive arrangement of the sonic crystals. In an attempt to physically realize this phenomenon, Farahat et al. (2008), have attempted to use a set of sonic crystals to yield anisotropic acoustic properties in water subject to low frequency surface waves. Their design was tailored to specific frequency and failed outside this very narrow band.

Using rigid-walled acoustic ducts with partial flexible panels on the other hand was investigated by several researchers targeting effective passive noise control techniques. This was achieved in 1D continuous domains by varying the stiffness of the waveguide through which the propagation takes place at certain locations, yielding added acoustic impedance that affects the overall propagation pattern inside the wave guide. For example, in 1999, Huang developed a theoretical analysis of a 1D rigid duct with partial flush-mounted flexible panels in an attempt to passively control the noise inside the duct. It was found that for a plane sound wave traveling in the flexible segment, the wall compliance renders a wave speed less than the speed of sound in air. For panels with substantial structural damping, both flexural and sound waves diminish with distance, eliminating the acoustic pass bands noticed with rigid walled duct. Huang et al. (2000) have also studied experimentally the sound propagation in 1D rigid ducts with partially flexible walls to investigate the coupling nature between the fluid domain and the flexible parts of the duct. He also investigated the effect of the compliance of flexible membranes covering parts of the rigid duct on the transmission loss. In 2002, Huang also conducted a modal analysis of a drum-like silencer. Similar analysis was conducted by Choi and Kim (2002), where they showed that supersonic fluid-dominant waves and subsonic membrane-dominant waves exist and that the latter provides powerful mechanism of transmission loss through the membrane damping and destructive reflections at the edges of the membrane maintaining a uniform cross-sectional area. In 2006, Chiu et al. studied the effect of magnetic forces on a drum-like silencer in pressurized cavities. In all these attempts, the researchers were interested in imposing additional impedance on the acoustic domain in order to improve the transmission loss inside an acoustic duct, very similar to the effect of Helmholtz resonators. The impedance mismatch zones were either tuned at specific frequencies, or controlled using various techniques. Such techniques were mainly focusing on changing the volume of the resonator, either by using mechanical, hydraulic or electrical circuits (Izumi et al., 1991; von Flotow et al., 1994; Esteve and Johnson, 2005). Fang et al. (2006) and later Cheng et al. (2008) utilized arrays of Helmholtz resonators to develop cavities with negative bulk moduli.

In all the above studies, the focus has been placed on passive metamaterials with fixed material properties. This limits considerably the potential of these materials. In this article, the emphasis is placed on the development of a new class of 1D composite acoustic metamaterials with tunable effective bulk modulus, which can be tailored to have increasing or decreasing variation along the material volume. This is achieved by coupling an acoustic cavity with an array of Helmholtz resonators with flexible cavities rather than the standard rigid-cavity design. Controlling the compliance of the resonator wall affects significantly the coupling with the rest of the acoustic cavity system yielding a domain with tunable effective bulk modulus distribution.

This article is organized in to eight sections. In the first section, a brief introduction is presented. In the section 'Passive Helmholtz Resonator,' analysis of passive Helmholtz resonators and their equivalent electrical analogy and the corresponding effective bulk modulus when coupled to an acoustic cavity are introduced. In the 'Active Helmholtz Resonator' section, lumped-parameter model for a cavity coupled to a Helmholtz resonator with flexible piezoelectric diaphragm is outlined in order to motivate the need for the active component to achieve a *programmable* acoustic metamaterial. In the section 'Programmable Effective Bulk Modulus,' the analysis for a *programmable* bulk modulus is presented. In the 'Error Analysis' section, error analysis for using long wavelength assumption at higher frequencies and larger cavity dimensions is provided. In the section 'Multi-cavities Coupled with Active Helmholtz Resonators,' the equations for a composite active acoustic metamaterial consisting of coupled acoustic cavities are presented. In the section 'Stability for the Piezoelectric Diaphragm,' the stability margins for the piezoelectric boundaries are calculated. A brief summary of the conclusions and the future work are outlined in the last section.

PASSIVE HELMHOLTZ RESONATOR

Adding Helmholtz resonators to acoustic cavities has proven to be effective in minimizing the acoustic energy and maximizing the transmission loss at certain narrow band of frequencies, which coincides with the natural frequency of the Helmholtz resonator. Coupling a Helmholtz resonator to an acoustic cavity as shown in Figure 1(a), results in a coupling mechanism between both the cavity and the resonator that would yield an effective bulk modulus for the combined system, which can be evaluated using the electrical-acoustic analogy circuit shown in Figure 2.

For proper modeling the main acoustic cavity is divided into two equal sections with the resonator coupled in between as shown in Figure 1(b).

The acoustic mass and stiffness in each cavity section is represented by the inductor $L_F = \rho_f L/A$ and capacitor $C_F = AL/B_f$. The Helmholtz resonator mass $M_H = \rho_f \times l \times a$ and stiffness $K_H = B_f a^2/(A_H \times l_H)$ are represented by suitable inductor and capacitor, respectively (Rossing, 2007).

From the circuit presented in Figure 2, the effective bulk modulus for the cavity can be calculated by considering volumetric rate of change of the acoustic cavity, which is ideally represented by the loops with Q and Q_1. Hence, the rate of change in the acoustic pressure is given as:

$$\dot{P} = -B_e \frac{Q - Q_H}{2AL}, \tag{1}$$

where B_e is the effective bulk modulus and Q_H is the acoustic volume flow rate in the Helmholtz resonator domain.

To calculate the effective bulk modulus for the cavity system B_e, the electrical impedance of the second half of the cavity Z_2 and that of the Helmholtz resonator Z_H are coupled with the electric circuit representing the first half of the cavity as follows:

$$Z_2 = \frac{\rho_f L s}{A} + \frac{B_f}{ALs} = \frac{1}{ALs}\left(B_f + \rho_f L^2 s^2\right), \tag{2}$$

$$Z_H = \frac{1}{a^2 s}\left(K_H + M_H s^2\right). \tag{3}$$

Hence, the total impedance of the system is calculated as:

$$Z_t = \frac{Z_2 Z_H Z_{CF}}{Z_2 Z_H + Z_H Z_{CF} + Z_{CF} Z_2} + Z_{LF}, \tag{4}$$

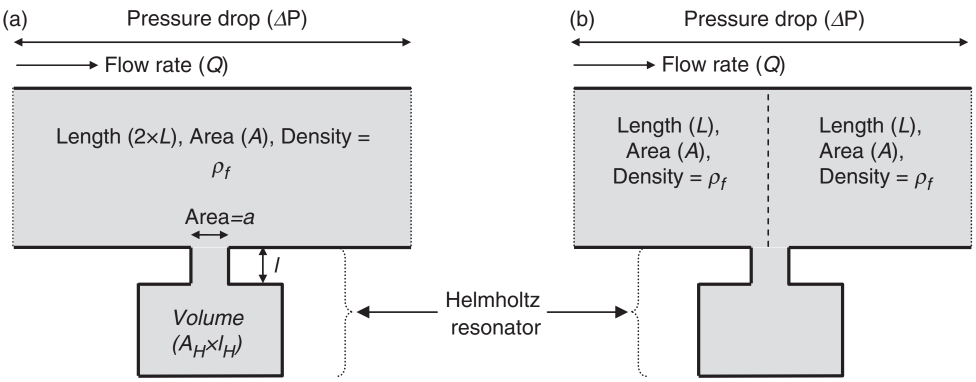

Figure 1. *Helmholtz resonator coupled to an acoustic cavity: (a) single main acoustic cavity, (b) cavity divided in two equal sections.*

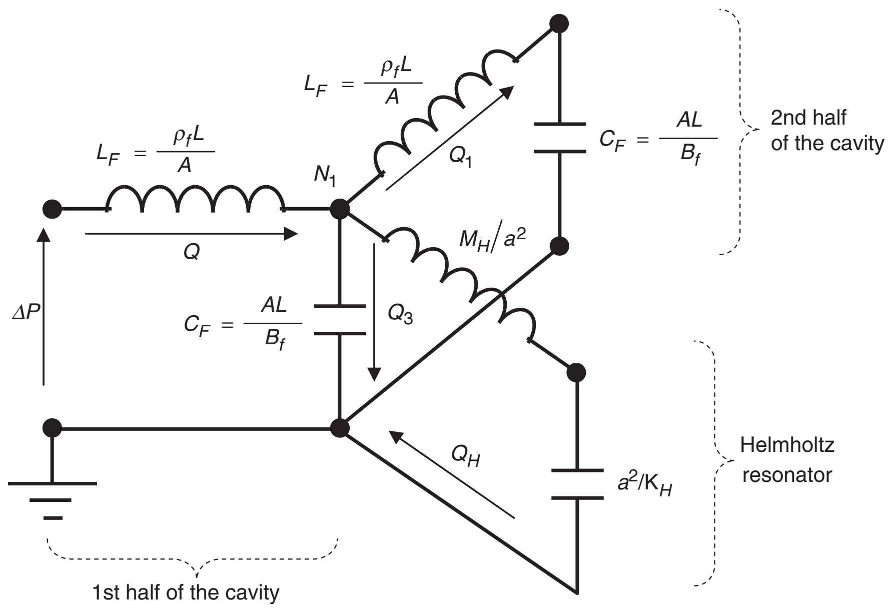

Figure 2. *Electrical circuit analogy of an acoustic cavity coupled with a Helmholtz resonator.*

with

$$Z_{CF} = \frac{1}{C_F s}, \quad Z_{LF} = L_F s = \frac{B_f L s}{A c_f^2}, \tag{5}$$

where c_f is the nominal speed of sound in the acoustic cavity.

Substituting Equations (2), (3), and (5) into Equation (4), yields:

$$Z_t = \frac{\dfrac{1}{a^2 A^2 L^2 s^3}\left[B_f\left(K_H + M_H s^2\right)\left(B_f + \rho_f L^2 s^2\right)\right]}{\dfrac{1}{a^2 A^2 L^2 s^2}\left[\begin{array}{c} B_f\left(B_f + \rho_f L^2 s^2\right)a^2 + B\left(K_H + M_H s^2\right) \\ AL + \left(K_H + M_H s^2\right)\left(B_f + \rho_f L^2 s^2\right)AL \end{array}\right]} + \frac{B_f L s}{A c_f^2}. \tag{6}$$

As $c_f = \sqrt{B_f/\rho_f}$, then Equation (6) reduces to:

$$Z_t = \frac{\left[B_f^2\left(K_H + M_H s^2\right)\left(1 + \frac{L^2 s^2}{c_f^2}\right)\right]}{s\left[\begin{array}{c} B_f^2\left(1 + \frac{L^2 s^2}{c_f^2}\right)a^2 + B_f\left(K_H + M_H s^2\right) \\ AL + B_f\left(K_H + M_H s^2\right)\left(1 + \frac{L^2 s^2}{c_f^2}\right)AL \end{array}\right]} + \frac{B_f L s}{A c_f^2}. \tag{7}$$

Since we are assuming that the spatial parameters of the encountered cavities must be very small compared to the acoustic wavelength, $(L^2 s^2/c_f^2) \ll 1$, Equation (7) reduces to:

$$Z_t = \frac{\left[B_f\left(K_H + M_H s^2\right)\right]}{s\left[B_f a^2 + \left(K_H + M_H s^2\right)AL + \left(K_H + M_H s^2\right)AL\right]} + \frac{Ls}{A c_f^2}. \tag{8}$$

Hence, the acoustic volume flow rate in the acoustic cavity with the Helmholtz resonator is defined as:

$$Q = \frac{P}{Z_t}. \tag{9}$$

The pressure at node N_1, shown in Figure 2, is calculated as:

$$P_1 = P\left(1 - \frac{Z_{LF}}{Z_t}\right). \tag{10}$$

Since the acoustic cavity is defined by the regions shown in Figure 1(b) without the Helmholtz resonator, then the volume flow rate within the cavity domain is defined as:

$$Q - Q_H = P\left(\frac{Z_H - Z_t + Z_{LF}}{Z_t Z_H}\right). \tag{11}$$

From Equations (1) and (11), B_e is calculated as:

$$B_e = B_f\left(1 + \left(\frac{2L^2 s^2}{c_f^2} + \frac{a^2 L B_f s^2}{c_f^2 A(K_H + M_H s^2)}\right)\right). \tag{12}$$

Note that the above for the effective bulk modulus is calculated without adding any damping in the system. When damping due to dissipative losses in the Helmholtz resonator is added, the frequency-dependent effective bulk modulus is shown in Figure 3. The displayed response is in agreement with the results reported by Fang et al. (2006).

ACTIVE HELMHOLTZ RESONATOR

As seen from Equation (12), the effective bulk modulus for the acoustic cavity depends on the Helmholtz resonator parameters. Therefore, controlling these parameters will affect the effective bulk modulus for the acoustic cavity to yield any prescribed value. The control of the Helmholtz resonator takes place by coupling the resonator cavity with a piezoelectric diaphragm as shown in Figure 4. Applying external voltage to the diaphragm will change its effective stiffness and accordingly the overall or effective bulk modulus of the acoustic cavity/resonator system. The analogous electrical circuit for the cavity coupled with the active Helmholtz resonator is shown in Figure 5.

Piezoelectric Equations

Consider the Helmholtz resonator with piezoelectric diaphragm shown in Figure 6.

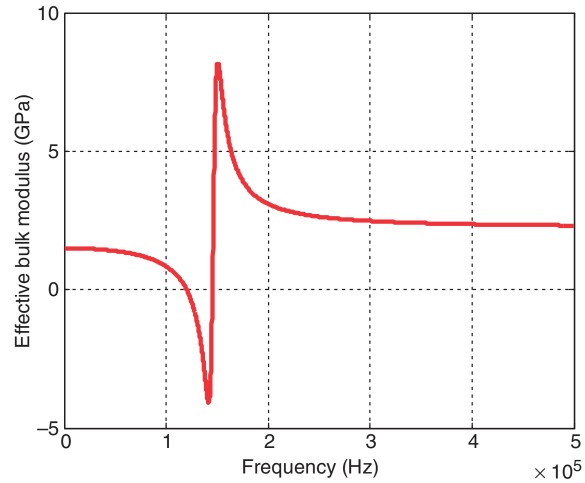

Figure 3. Frequency-dependent effective bulk modulus.

The basic constitutive equation for a piezoelectric material is given by:

$$\begin{Bmatrix} S \\ D \end{Bmatrix} = \begin{bmatrix} s^E & d \\ d & \varepsilon \end{bmatrix} \begin{Bmatrix} T \\ E \end{Bmatrix}, \tag{13}$$

where S = strain, D = electrical displacement, T = stress, E = electrical field, s^E = compliance, d = piezoelectric strain coefficient, and ε = permittivity. Equation (13) can be rewritten as:

$$\begin{Bmatrix} \Delta \mathrm{Vol} \\ q \end{Bmatrix} = \begin{bmatrix} C_D & d_A \\ d_A & {}^1\!/_{Z_p s} \end{bmatrix} \begin{Bmatrix} \Delta P_p \\ V_p \end{Bmatrix}, \tag{14}$$

where $\Delta\mathrm{Vol}$ = change in diaphragm volume, q = electrical charge, ΔP_p = pressure across piezo-diaphragm, and V_p = voltage. Also, C_D = diaphragm compliance = A_H^2/K_D, K_D = diaphragm stiffness and Z_P = impedance of piezo-diaphragm and attached elements given by:

$$Z_p = \frac{L_P s}{1 + L_P\left(\dfrac{C_P C_s}{C_P + C_s}\right)s^2}, \tag{15}$$

where C_P = capacitance of piezo-diaphragm = $A_H\varepsilon/l_p$ with A_H = diaphragm area, l_p = diaphragm thickness. Also, L_P denotes a shunted inductance in-parallel with the piezo-diaphragm, and C_s denotes a capacitance in-series with the piezo-diaphragm.

The electric circuit analogous to the resonator cavity coupled with a piezoelectric diaphragm is as shown in Figure 7.

Using the piezo-diaphragm as a self-sensing actuator, then the second row of Equation (14) gives, for a short-circuit piezo-sensor, the following expression:

$$q = d_A \Delta P_p. \tag{16}$$

Then, the voltage V_p applied to the piezo-diaphragm can be generated by a direct feedback of the charge q such that:

$$V_p = -G\,\mathrm{d}A\,\Delta P_p, \tag{17}$$

where G = feedback gain.

Then, the first row of Equation (14) yields:

$$\Delta \mathrm{Vol} = \left(C_D - d_A^2 G\right)\Delta P_p = C_{DC}\Delta P_p, \tag{18}$$

where C_{DC} = closed-loop compliance of piezo-diaphragm.

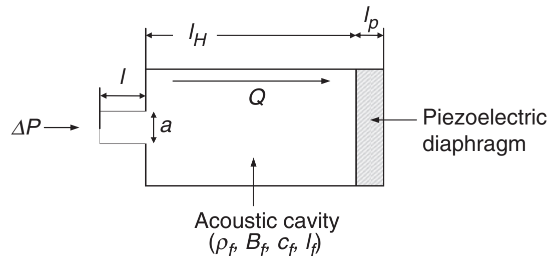

Figure 6. *Helmholtz resonator coupled with a piezoelectric diaphragm.*

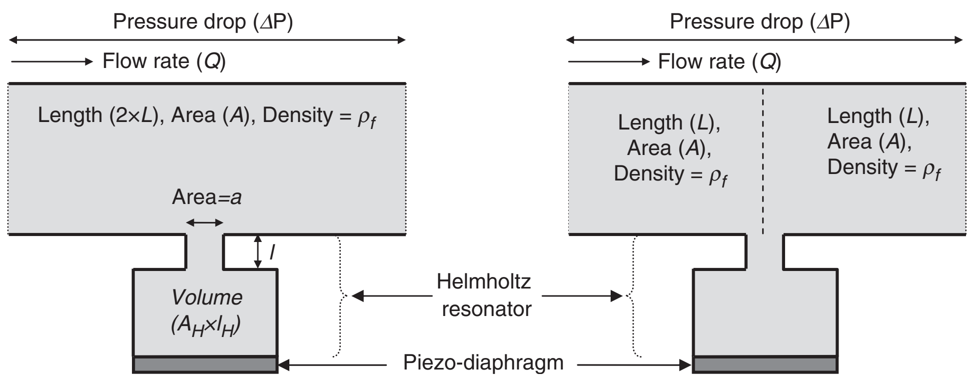

Figure 4. *Acoustic cavity coupled with active Helmholtz resonator.*

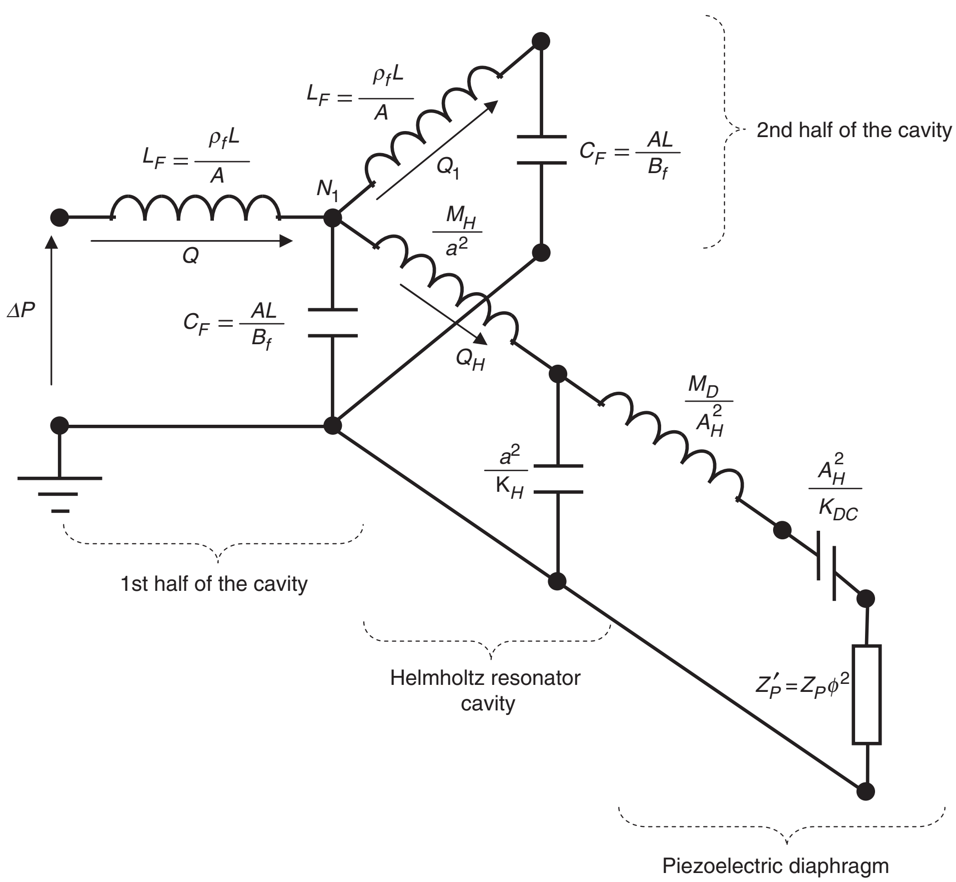

Figure 5. *Electrical circuit analogous to a cavity coupled with an active Helmholtz resonator.*

Hence, the circuit in Figure 7 is reduced to that shown in Figure 8.

Basic Electrical-Acoustic Equations

To calculate the effective bulk modulus B_e for the cavity system, the electrical impedance of the second half of the cavity Z_2 and that of the active Helmholtz resonator Z_H are coupled with the electric circuit representing the first half of the cavity as follows:

$$Z_2 = Z_{CF} + Z_{LF}, \tag{19}$$

$$Z_H = \frac{(Z_{LD} + Z_{CDC} + Z'_P)Z_{CH}}{Z_{LD} + Z_{CDC} + Z'_P + Z_{CH}} + Z_{LH}, \tag{20}$$

where

$$Z_{CF} = \frac{1}{C_F s} = \frac{B_f}{ALs}, \tag{21a}$$

$$Z_{LF} = L_F s = \frac{\rho_f L s}{A}, \tag{21b}$$

$$Z_{CH} = \frac{K_H}{a_H^2 s}, \tag{21c}$$

$$Z_{LH} = \frac{M_D s}{a_H^2}, \tag{21d}$$

$$Z_{CDC} = \frac{K_{DC}}{A_H^2 s}, \tag{21e}$$

$$Z_{LD} = \frac{M_D s}{A_H^2}, \tag{21f}$$

$$Z'_P = Z_P\phi^2 = \frac{L_P s}{1 + L_P\left(\frac{C_P C_s}{C_P + C_s}\right)s^2}\phi^2, \tag{21g}$$

where, ϕ is the volt/pressure conversion factor for the piezoelectric diaphragm.

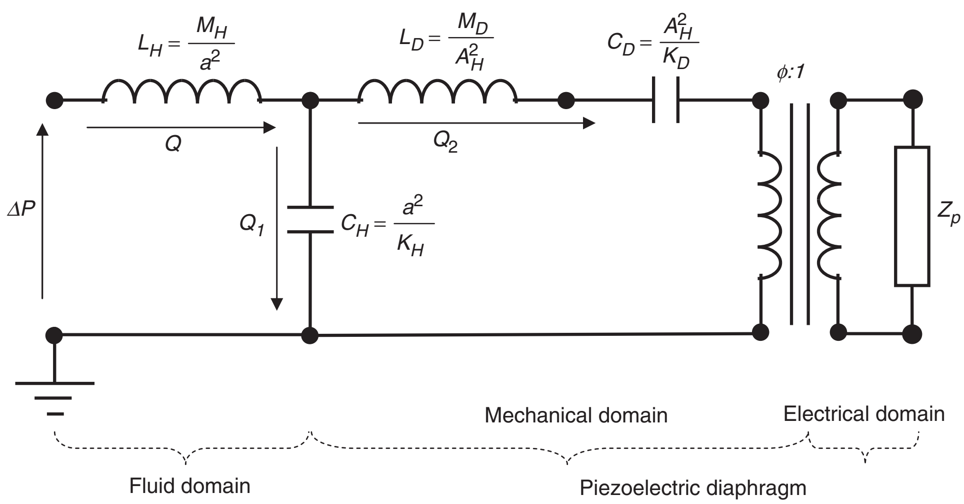

Figure 7. *Electrical analog for the Helmholtz resonator coupled with open-loop piezoelectric diaphragm.*

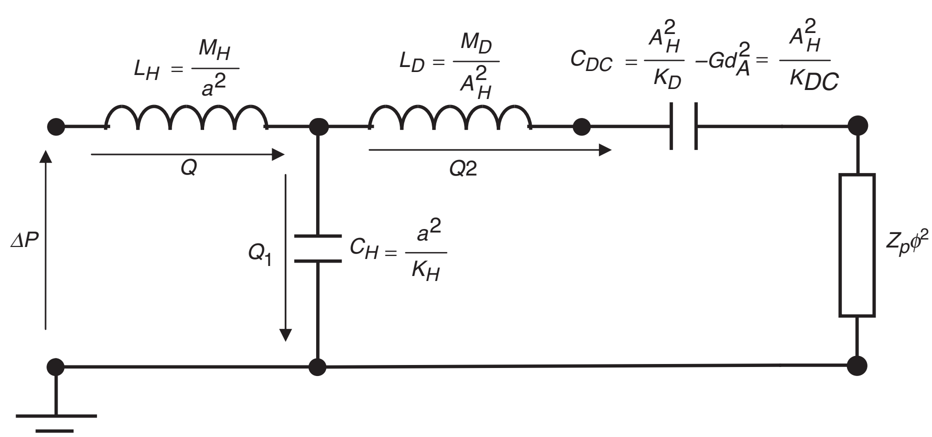

Figure 8. *Electrical analog for an acoustic fluid domain coupled with closed-loop piezoelectric diaphragm.*

Substituting the identities defined in Equations (21) into (19) and (20) results in:

$$Z_2 = \frac{1}{ALs}\left(B_f + \rho_f L^2 s^2\right), \tag{22}$$

$$Z_H = \frac{M_H s}{a^2} + \frac{K_H\left(K_{DC} + s(M_D s + A_H^2 Z'_P)\right)}{s\left(A_H^2 K_H + a^2\left(K_{DC} + s\left(M_D s + A_H^2 Z'_P\right)\right)\right)}. \tag{23}$$

Therefore and taking advantage of long wavelength assumption, the total impedance of the system is calculated as:

$$Z_t = \frac{Z_2 Z_H Z_{CF}}{Z_2 \times Z_{CF} + Z_H \times Z_{CF} + Z_2 \times Z_H} + Z_{LF} = \frac{M_H s}{a^2} + \frac{C_1}{C_2 + C_3 + C_4}, \tag{24}$$

$$Z_t = \frac{B_f L s}{A c_f^2} + \frac{B_f c_f^2 \begin{pmatrix} A_H^2 K_H M_H s^2 + a^2\left(K_H + M_H s^2\right) \\ \left(K_{DC} + M_D s^2 + A_H^2 s Z'_P\right) \end{pmatrix}}{s\begin{pmatrix} A A_H^2 K_H L M_H s^2 2 c_f^2 + a^2 c_f^2\left(K_{DC} + M_D s^2 + A_H^2 s Z'_P\right) \\ \left(a^2 B_f + 2AL\left(K_H + M_H s^2\right)\right) + a^2 A_H^2 B_f K_H c_f^2 \end{pmatrix}}. \tag{25}$$

Following Equations (9)–(11), utilizing the definition for the effective bulk modulus in (1) and the long wavelength assumption, B_e is given as:

$$B_e = 2ALs\left(\frac{Z_t Z_H}{Z_H - Z_t + Z_{LF}}\right), \tag{26}$$

$$B_e = B_f\left[1 + \frac{B_f L a^2 s^2\left(\left(K_{DC} + MDs^2 + A_H^2 s Z'_P\right)a^2 + K_H A_H^2\right)}{A c_f^2 \begin{pmatrix} A_H^2 K_H M_H s^2 + a^2\left(K_H + M_H s^2\right) \\ \left(K_{DC} + MDs^2 + A_H^2 s Z'_P\right) \end{pmatrix}}\right]. \tag{27}$$

PROGRAMMABLE EFFECTIVE BULK MODULUS

In order to maintain a prescribed effective bulk modulus B_e for the cavity over a wide frequency range, the stiffness of the piezoelectric diaphragm has to be controlled. Taking advantage of the long wavelength assumption and defining $B_r = B_e/B_f$, solving Equation (27) for K_{DC}, results in:

$$K_{DC} = \frac{\begin{pmatrix} A A_H^2 (B_r - 1) c_f^2 K_H M_H s^2 + \left(M_D s^2 + A_H^2 s Z'_P\right) \\ \times\left(a^2 A (B_r - 1) c_f^2\left(K_H + M_H s^2\right) - a^4 B_f L s^2\right) \\ -a^2 B_f K_H L A_H^2 s^2 \end{pmatrix}}{a^2\left(a^2 B_f L s^2 - A(B_r - 1)c_f^2 (K_H + M_H s^2)\right)}. \tag{28}$$

The gain (G) for the piezoelectric controller is calculated from Equation (18) such that:

$$G = \frac{1}{d_A^2}\left(C_D - \frac{A_H^2}{K_{DC}}\right) = \frac{A_H^2}{d_A^2}\left(\frac{1}{K_D} - \frac{1}{K_{DC}}\right). \tag{29}$$

Figure 9(a)–(c) shows the resultant relative bulk modulus, piezo-diaphragm stiffness, and the control voltage and for $B_r = 20$, respectively. Figure 9(d) shows the uncontrolled relative bulk modulus for the same cavity configuration.

ERROR ANALYSIS

By increasing the acoustic frequency, the effect of the terms encountering $L^2 s^2 / c_f^2$ starts to become significant, especially for small prescribed effective bulk modulus B_e. Therefore, if one is applying those approximations, one should be aware of the encountered approximation errors. The frequency-dependent effective bulk modulus for a cavity length of 1 cm using exact formulation and with long wavelength assumption approximation is shown in Figure 10.

The approximations adopted in calculating the closed-loop piezoelectric stiffness K_{DC} or compliance C_{DC} that would yield a prescribed value for the effective bulk modulus for the main acoustic cavity B_e suffers significantly at higher frequencies and for small values of B_e. Results for approximate and exact models for a cavity of 1 cm length are compared and the percentage error are illustrated in Figures 11 and 12 for prescribed values of B_r of 20 and 0.04, respectively. In Figure 13, the same comparison is conducted for a cavity length of 2 mm and a value of B_r of 0.04.

MULTI-CAVITIES COUPLED WITH ACTIVE HELMHOLTZ RESONATORS

In this section, the performance of multi-cell acoustic metamaterial as shown in Figure 14 is considered. Each cell consists of a single acoustic cavity coupled with a single active Helmholtz resonator. The coupling between the adjacent cells must be taken into consideration, as the effect of changing the bulk modulus B_e for each cell would certainly affect the neighboring cells and its neighboring fluid cavities. The electrical analogous circuit for the system of N cells is illustrated in Figure 15.

In the system of N cascading acoustic cells, the last cell represents the cell subject to external pressure excitation, while the first one is the end of the chain of the cascading cells. Due to the coupling nature of the cells, a recursive solution pattern has to be adopted in order to calculate the different stiffness values of the piezoelectric diaphragms K_{DCi} needed to ensure a prescribed set of effective bulk's moduli within the cascading coupled cells.

The recursive approach starts with the first cell, which is coupled from one side only to the rest of the cells.

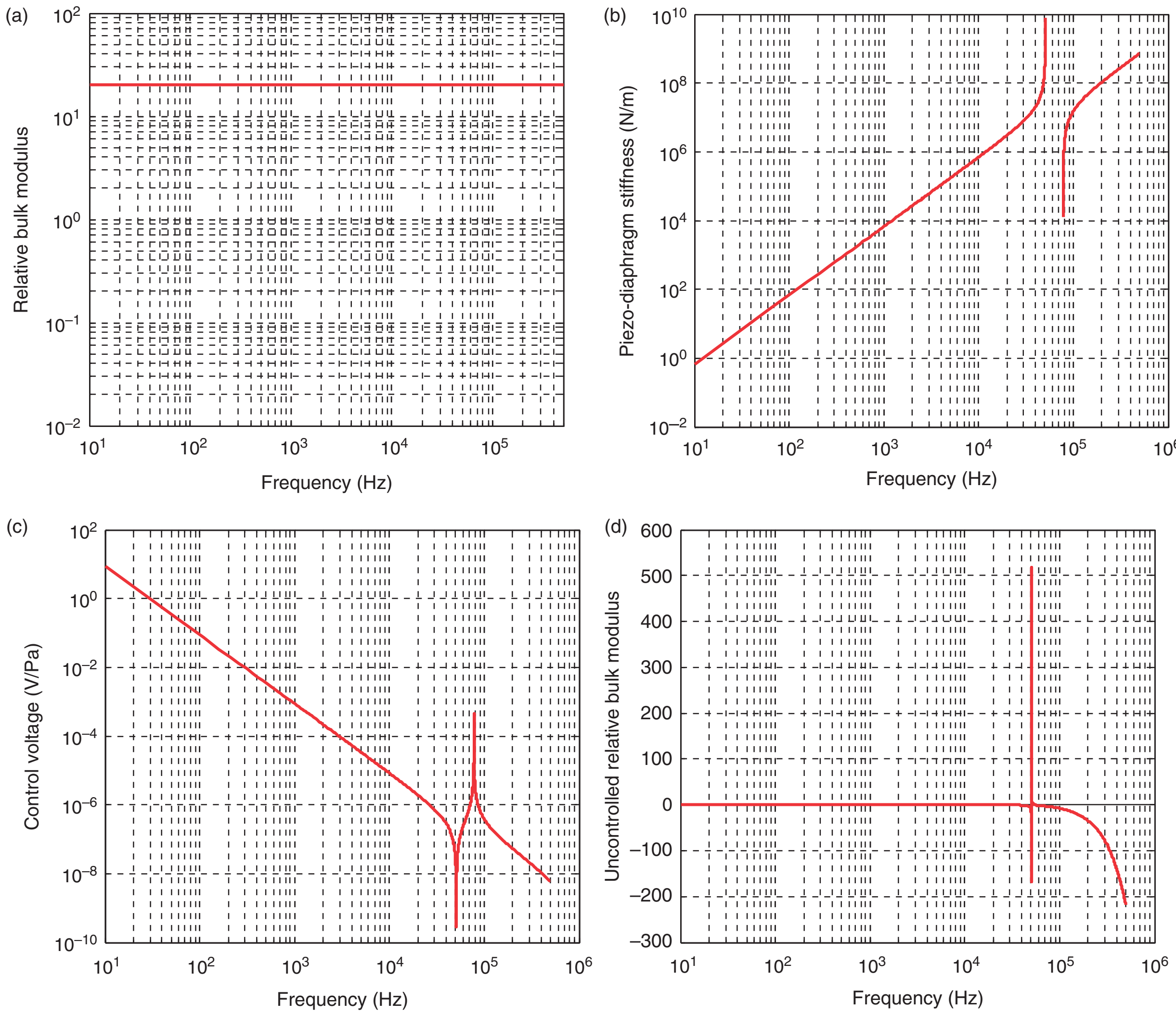

Figure 9. *Comparison between controlled and uncontrolled effective cavity bulk modulus for $B_r = 20$: (a) resultant relative bulk modulus, (b) resultant piezo-diaphragm stiffness, (c) control voltage, (d) uncontrolled relative bulk modulus.*

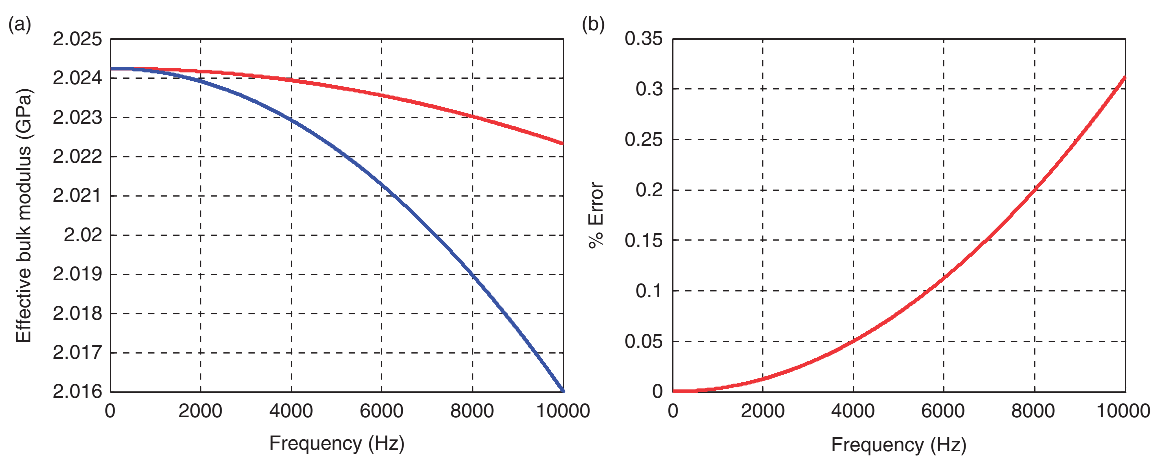

Figure 10. *Frequency-dependent effective bulk modulus (— exact, — approximate): (a) exact vs approximate calculation, (b) percentage error due to approximation.*

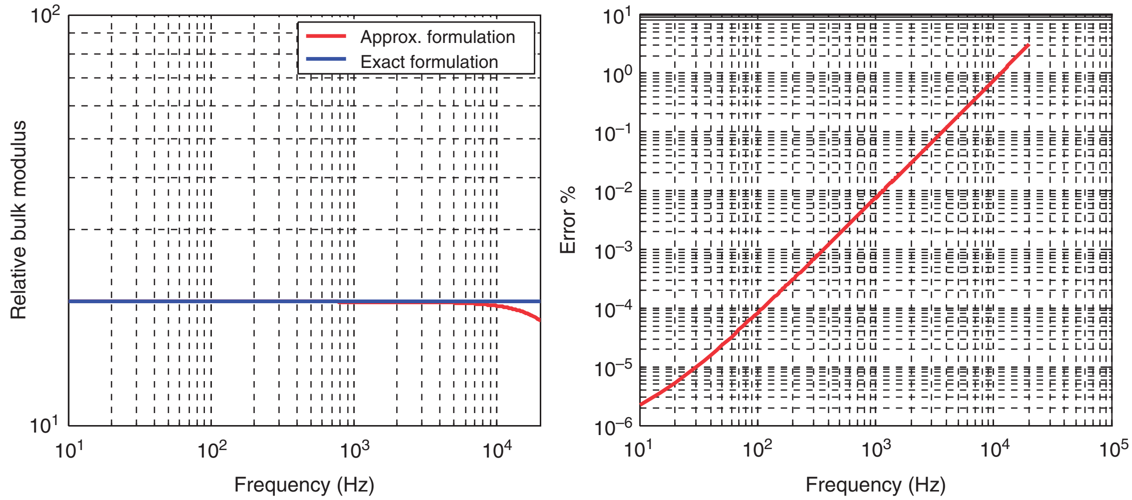

Figure 11. *B_e calculation using approximate and exact models ($B_r = 20$), $L = 1$ cm.*

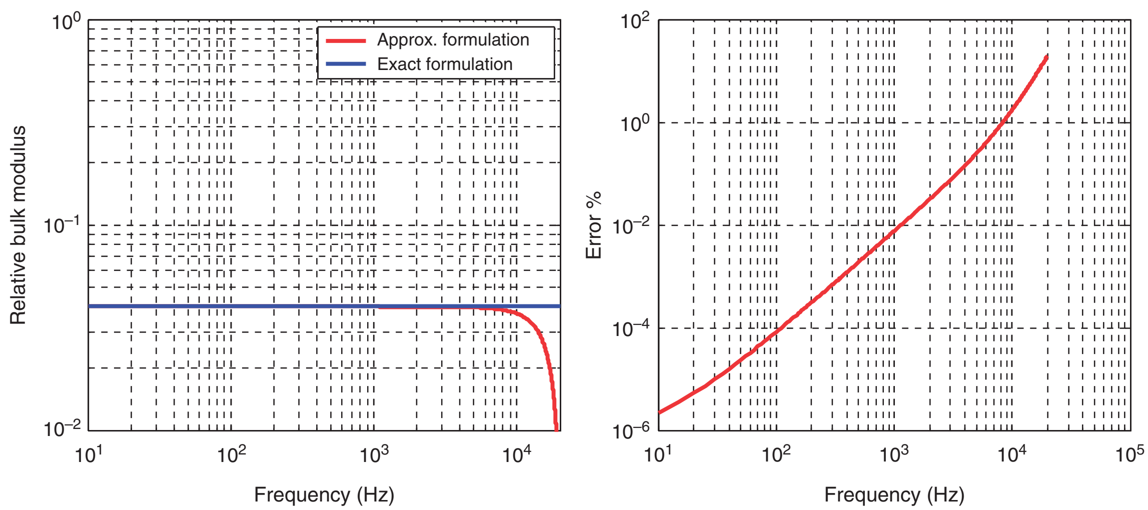

Figure 12. *B_e calculation using approximate and exact models ($B_r = 0.04$), $L = 1$ cm.*

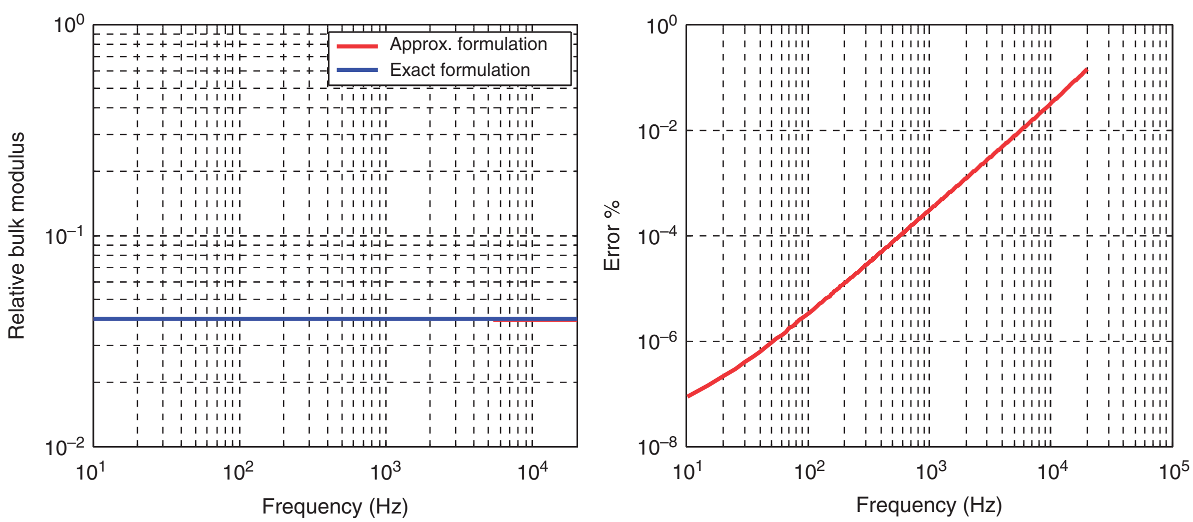

Figure 13. *B_e calculation using approximate and exact models ($B_r = 0.04$), $L = 2$ mm.*

Using the electrical analogy, the overall impedance Z_1 of this cell can be calculated as a function of the piezoelectric stiffness K_{DC1} and the required effective bulk modulus B_{e1} as given by Equations (25)–(28). Once calculated, this impedance is shunted to the circuit representing the rest of the chain. Hence the second cell, loaded with the impedance of the first cell, is now the end of the chain of cells, and is coupled to the rest of the cells from one side only. Again using the electrical analogy, the overall impedance Z_2 of the first two cells can be calculated as a function of the piezoelectric diaphragm stiffness K_{DC2} and the required effective bulk modulus B_{e2}. Following the same logic, the different stiffness values of the piezoelectric diaphragms K_{DCi} for the different cells that would yield the prescribed set of effective bulk's moduli can be obtained.

The electrical impedance of the first cell is calculated as in Equation (25), hence given by:

$$Z_1 = \frac{(Z_{LF}+Z_{CF})Z_{H1}Z_{CF}}{(Z_{LF}+Z_{CF})\times Z_{CF}+Z_{H1}\times Z_{CF}+(Z_{LF}+Z_{CF})\times Z_{H1}} + Z_{LF}. \tag{30}$$

The electrical impedance of the i-th cell is hence given as:

$$Z_i = \frac{\left(\frac{Z_{i-1}\times Z_{CF}}{Z_{i-1}\times Z_{CF}}+Z_{LF}\right)Z_{Hi}Z_{CF}}{\left(\frac{Z_{i-1}\times Z_{CF}}{Z_{i-1}\times Z_{CF}}+Z_{LF}\right)\times Z_{CF}+Z_{Hi}\times Z_{CF}+\left(\frac{Z_{i-1}\times Z_{CF}}{Z_{i-1}\times Z_{CF}}+Z_{LF}\right)\times Z_{Hi}} + Z_{LF}. \tag{31}$$

Following the same procedure as in (1) to (10), the effective bulk modulus B_{ei} for the i-th cell is hence given as:

$$B_{ei} = -\frac{sP_i \times (2 \times L \times A \times i)}{Q_i - Q_{Hi}}, \tag{32}$$

where P_i is the acoustic pressure at the entrance of the i-th cell, Q_i is the total acoustic volume flow rate in the whole i-th cell, Q_{Hi} is the acoustic volume flow rate in the flush-mounted panel in the i-th cell. Again, let $B_{ri} = B_{ei}/B_f$, then the value of the gain G_i is calculated from Equation (29) as:

$$G_i = \frac{1}{d_A^2}\left(C_D - \frac{A_H^2}{K_{DCi}}\right) = \frac{A_H^2}{d_A^2}\left(\frac{1}{K_D} - \frac{1}{K_{DCi}}\right). \tag{33}$$

Figure 16 presents a flow chart for the recursive process to calculate the values of K_{DCi} that would yield a set of prescribed values of B_{ei}.

Consider now an active acoustic metamaterial with characteristics as listed in Table 1. The metamaterial consists of eight cells. Four of these cells are programmed to generate material A with increasing density distribution while the remaining four are programmed to generate material B with decreasing density as shown in Figure 17. Figures 18–20 show the relative bulk modulus, the control voltage, and the stiffness of the piezoelectric diaphragms for the 8-cell system, respectively.

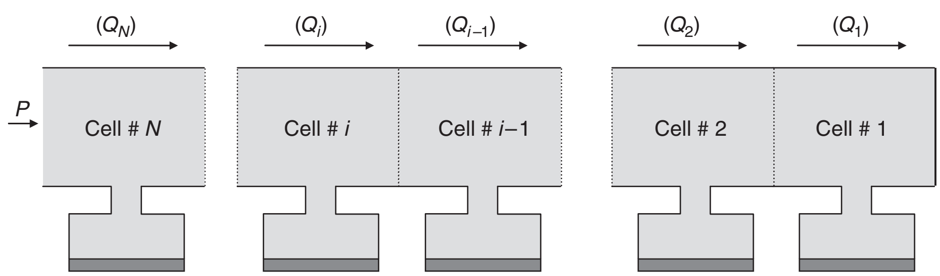

Figure 14. *A schematic for a set of N cascading and coupled cells.*

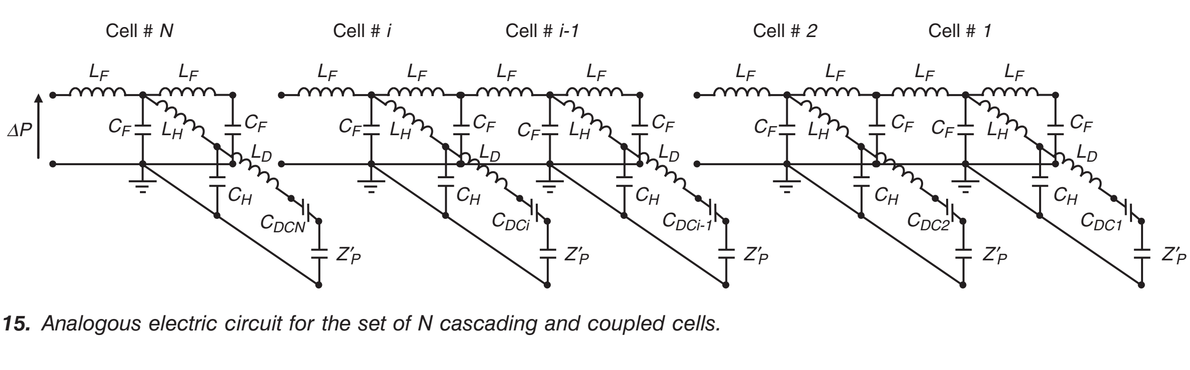

Figure 15. *Analogous electric circuit for the set of N cascading and coupled cells.*

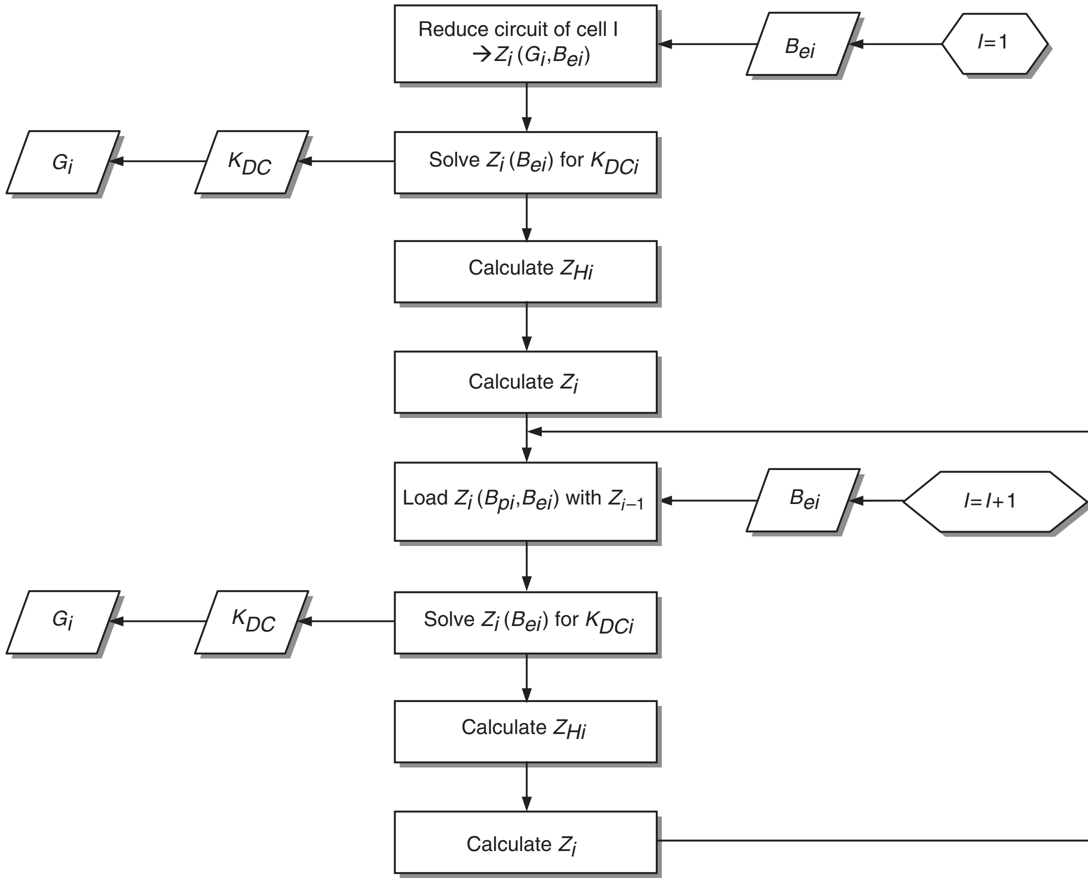

Figure 16. *Flowchart of the recursive algorithm.*

STABILITY FOR THE PIEZOELECTRIC DIAPHRAGM

In order to yield the prescribed effective bulk modulus for the cavity/resonators system, the stiffness of the piezoelectric diaphragm is tuned using a charge feedback control algorithm. This in turn changes the effective electromechanical stiffness of the piezoelectric diaphragm. For certain values of prescribed effective bulk modulus, the feedback control algorithm would result in an unstable mechanical system requiring a zero or even negative electromechanical stiffness of the piezo-element. In order to overcome this limitation a coupled inductor-in-parallel and a capacitor-in-series are connected to the piezoelectric diaphragm adding extra stiffness. The values for this set of capacitor-inductor are optimized to yield the required performance without crossing the stability boundary for the piezo-diaphragm. Hence, an integrated part of the analysis is to define the frequency stability margins for the system as a function of the capacitance and inductance coupled to the piezo-element. Another advantage of using the inductor-capacitor set is to reduce the control voltage needed to achieve the targeted effective bulk modulus of the acoustic cavity. This, however, is at the expense of the controller sensitivity towards different values of targeted effective bulk's moduli. To reach this objective, the equation describing the frequency-dependent stiffness of the piezoelectric diaphragm as a function of the capacitance and inductance, is equated to zero to yield the critical frequencies and define the legitimate frequency bands to operate within.

Table 1. Parameters of acoustic cavity/piezo-diaphragm system.

Parameter	Value
ϕ	138.3 (Pa/V)
B_D	200 (GPa)
ρ_D	7800 (kg/m^3)
C_P	21.155 (nF)
L	0.005 (m)
l_H	0.0025 (m)
l_p	0.00083 (m)
l	0.00125 (m)
a	1.56×10^{-6} (m^2)
A	25×10^{-6} (m^2)
A_H	11.1×10^{-6} (m^2)
d_A	$-170 \times 10^{-12} \times A_H$ (m^3/V)
ρ_f	1000 (kg/m^3)
B_f	2.25×10^9 (Pa)

Starting from Equation (30) and substituting for $Z'_P = (L_P s/1 + L_P C'_P s^2)\phi^2$ and $s = i\sqrt{\lambda}$, where $\lambda = \omega^2$

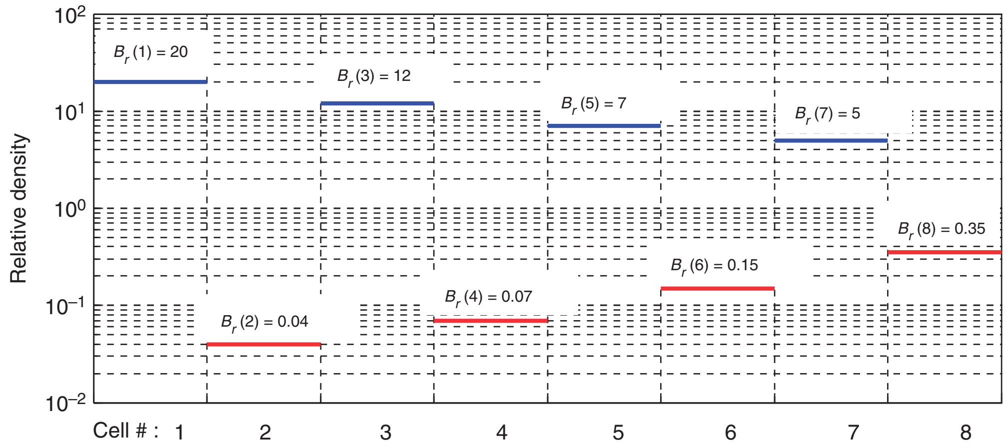

Figure 17. *Relative effective bulk modulus distribution for 8 cascading coupled cells.*

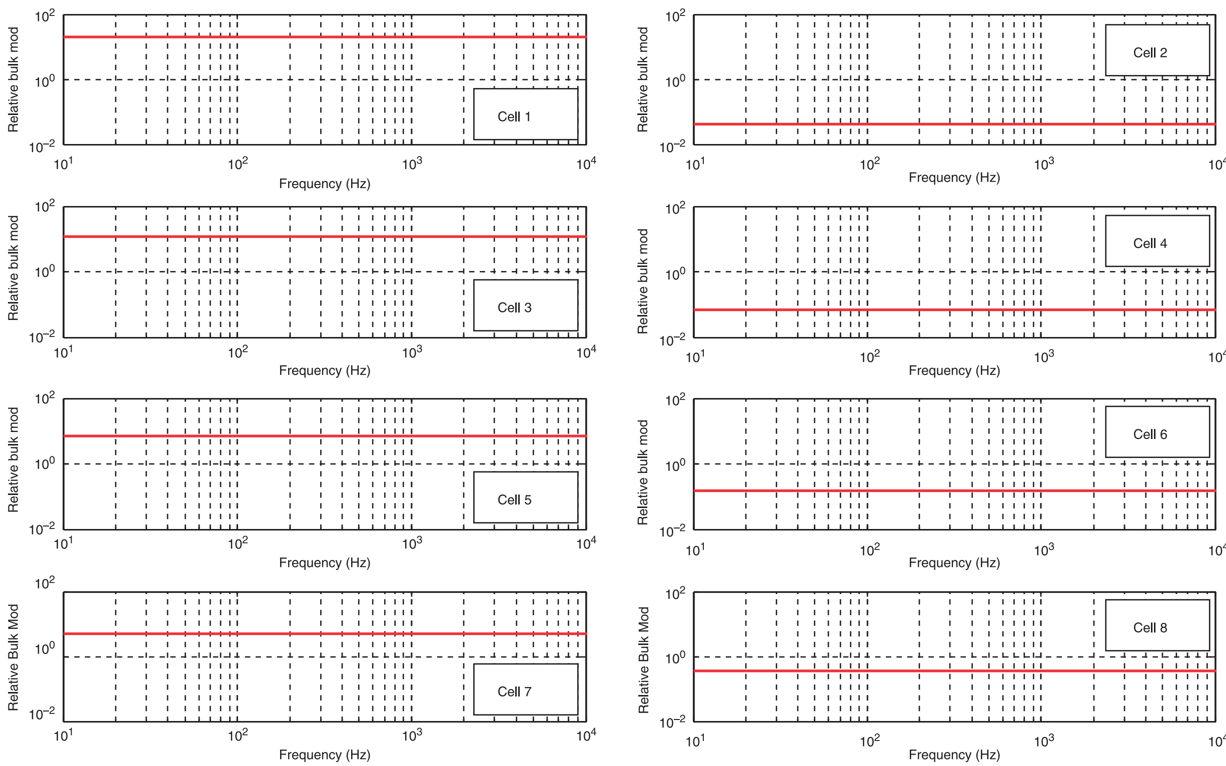

Figure 18. *Relative effective bulk modulus for the eight-cell system.*

(angular frequency of the excitation pressure) and C'_P is the effective capacitance of both the piezo-element and the added capacitor, K_{DC} is given as:

$$K_{DC} = \frac{\begin{pmatrix} AA_H^2(1-B_r)c_f^2K_HM_H\lambda^2 + \left(-M_D\lambda^2 + iA_H^2\lambda Z'_P\right) \\ \times\left(a^2A(B_r-1)c_f^2\left(K_H - M_H\lambda^2\right) + a^4B_fL\lambda^2\right) \\ +a^2B_fK_HLA_H^2\lambda^2 \end{pmatrix}}{a^2\left(-a^2B_fL\lambda^2 - A(B_r-1)c_f^2\left(K_H - M_H\lambda^2\right)\right)}. \tag{34}$$

Solving (34) for λ, yields two values at which the stiffness of the piezo-diaphragm becomes zero (λ_1 and λ_2). λ_1 and λ_2 are theoretically frequencies that we need to avoid in order to eliminate the possibility of unstable behavior for the piezo-diaphragm. However, from Equation (31) a resonance state occurs at:

$$\lambda_R = \frac{1}{C'_P L_P}, \tag{35}$$

which may limit the effective stability bandwidth if it lies below λ_1. In order to design a proper system, the

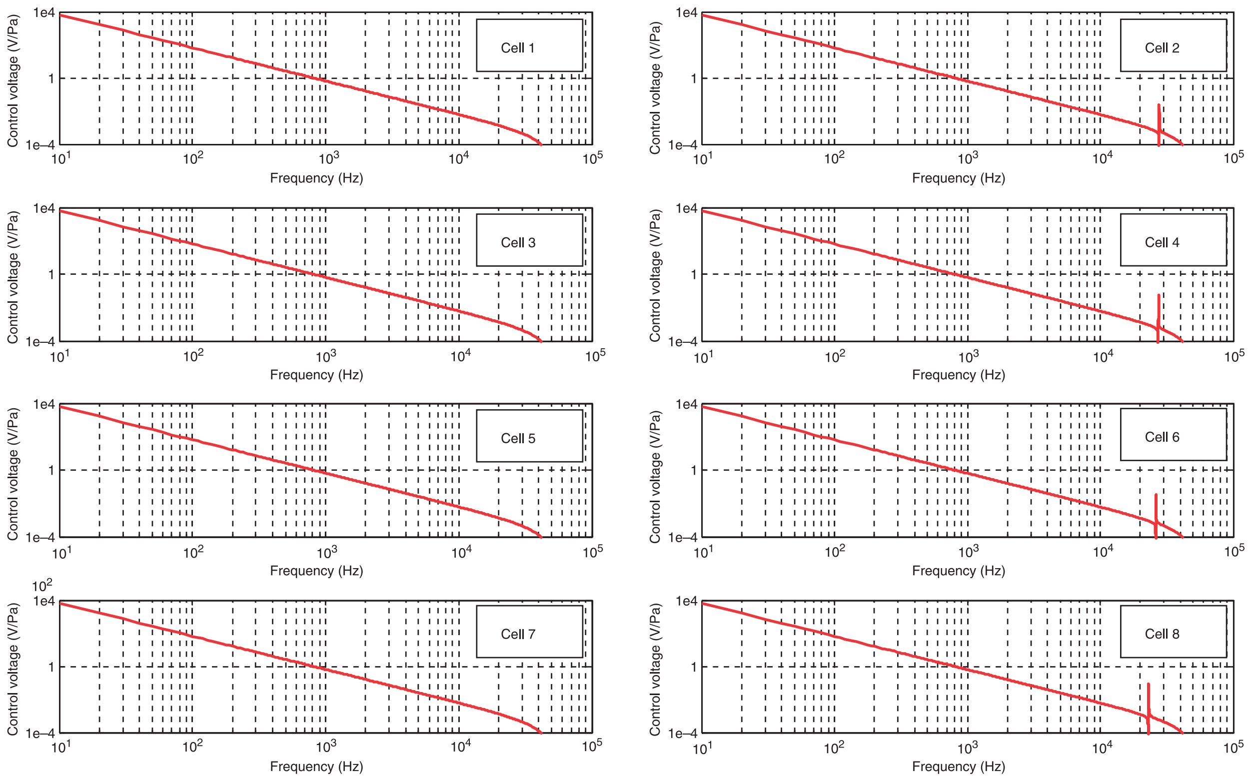

Figure 19. *Control voltage for the eight-cell system.*

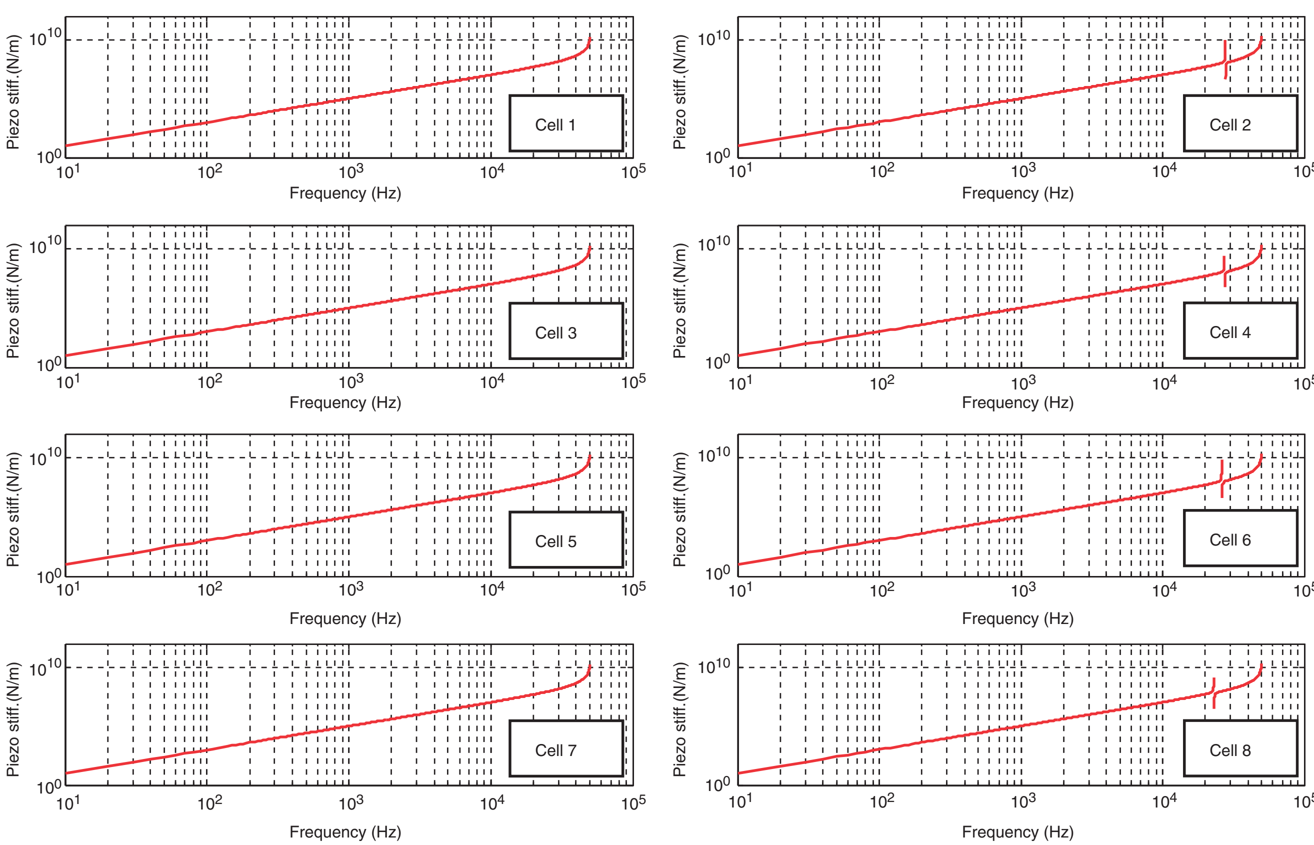

Figure 20. *Resultant piezo-diaphragm stiffness for the eight-cell system.*

minimum of the three frequencies must be larger than the maximum required excitation frequency. Figure 21(a) and (b) illustrate the effect of changing the inductance-in-parallel on the stability range and on the control voltage needed. Figure 22(a) and (b) illustrate the same effect for different values of the capacitance-in-series. In both cases, a bulk modulus of $B_r = 20$ is targeted.

As seen in Figures 21 and 22, increasing the inductance value would increase the stability region, but at the expense of the control voltage needed to achieve the desired effective bulk modulus. On the other hand, increasing the capacitance-in-series would lower the upper cut-off frequency of the stability range at the expense of the lower cut-off frequency producing a shift in the instability range towards the lower frequency zone, while maintaining the control voltage to moderate values.

CONCLUSIONS

This article has presented a new class of 1D acoustic metamaterials with *programmable* bulk modulus. The active metamaterials are shown theoretically to be tunable to have increasing or decreasing bulk modulus distributions along the material.

The theoretical analysis of this class of active acoustic metamaterials is presented for an array of cells consisting of water cavities coupled with flexible Helmholtz resonators that have piezoelectric boundaries. Various control strategies are considered to achieve different spectral and spatial control of the bulk modulus of this class of acoustic metamaterials. The theory presented is based on the lumped-parameter approach and the developed model is applied first to a single cell as well as arrangement of multi-cells. The presented results emphasize the potential of the active metamaterials for

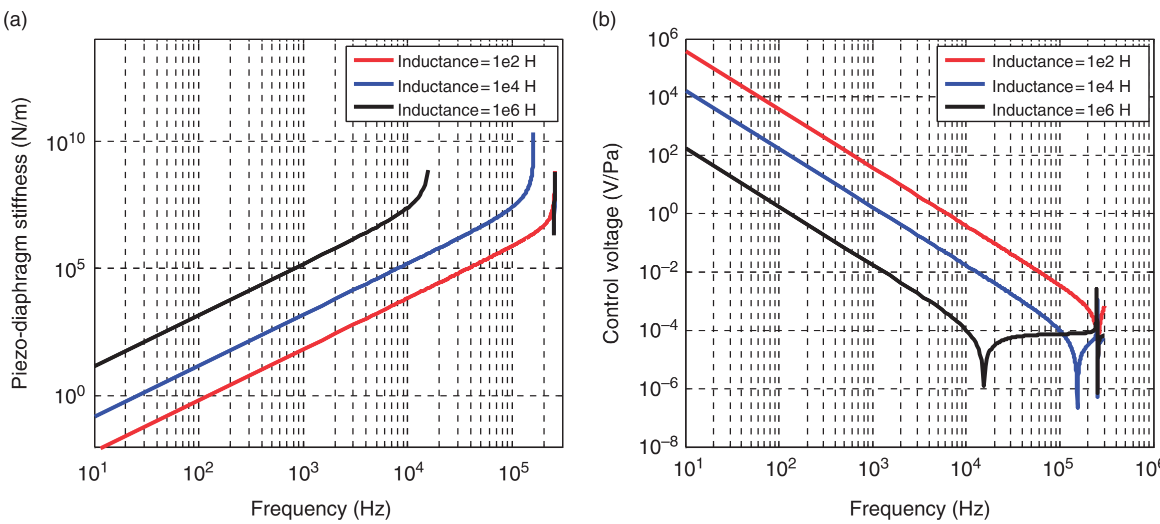

Figure 21. *Effect of the inductance-in-parallel on the piezo-diaphragm performance: (a) piezo-diaphragm stiffness (N/m), (b) control voltage (V/Pa).*

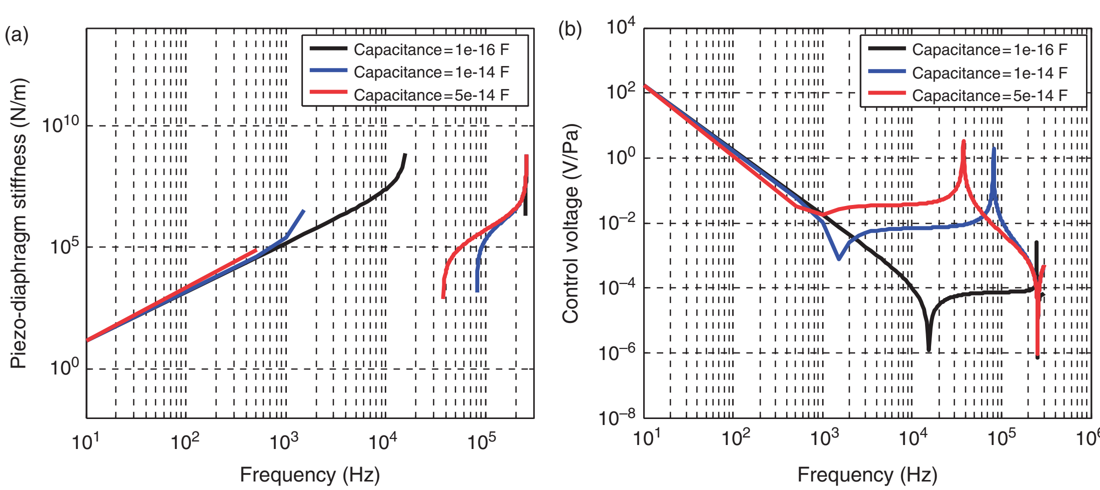

Figure 22. *Effect of the capacitance-in-series on the piezo-diaphragm performance: (a) piezo-diaphragm stiffness (N/m), (b) control voltage (V/Pa).*

physically generating a wide range of effective bulk's moduli in a simple and uniform manner.

Stability margins for the piezoelectric diaphragms are also investigated to outline the range of safe operation of the metamaterial. Furthermore, the effect of the design parameters of the metamaterial on the effective bandwidth is investigated.

Combining the tunable density and bulk modulus capabilities, will enable the physically realization of practical acoustic cloaks and objects treated with these active metamaterials can become acoustically invisible. Extension of the 1D acoustic metamaterials with tunable bulk modulus to 2D metamaterials is a natural extension of the present work.

ACKNOWLEDGMENTS

This work has been funded by a grant from the Office of Naval Research (N000140910038). Special thanks are due to Dr Kam Ng and Dr Scott Hassan, the technical monitors, for their invaluable input and comments.

REFERENCES

Cervera, F., Sanchis, L., Pérez, J., Sala, R., Rubio, C. and Meseguer, F. 2001. "Refractive Acoustic Devices for Airborne Sound," *Physical Review Letters*, 88(2):023902-1–023902-4.

Chan, C.T., Jensen, L.I. and Fung, K.H. 2006. "On Extending the Concept of Double Negativity to Acoustic Waves," *Journal of Zhejiang University Science A*, 7(1):24–28.

Cheng, Y., Yang, F., Xu, J. and Liu, X. 2008. "A Multilayer Structured Acoustic Cloak with Homogeneous Isotropic Materials," *Applied Physics Letters*, 92(15):151913-1–151913-3.

Chiu, Y.H., Cheng, L. and Huang, L. 2006. "Drum-like Silencers using Magnetic Forces in a Pressurized Cavity," *Journal of Sound and Vibration*, 297:895–915.

Choia, S. and Kim, Y. 2002. "Sound-wave Propagation in a Membrane–duct (L)," *Journal of the Acoustical Society of America*, 112(5):1749–1752.

Cummer, S., Popa, B., Schurig, D., Smith, D., Pendry, J., Rahm, M. and Starr, A. 2008b. "Scattering Derivation of a 3D Acoustic Cloaking Shell," *Physics Review Letters*, 100(2):024301-1–024301-4.

Cummer, S., Rahm, M. and Schurig, D. 2008a. "Material Parameters and Vector Scaling in Transformation Acoustics," *New Journal of Physics*, 10:115025-1–115025-12.

Cummer, S. and Schurig, D. 2007. "One Path to Acoustic Cloaking," *New Journal of Physics*, 9:1–8.

Ding, Y., Liu, Z., Qiu, C. and Shi, J. 2007. "Metamaterial with Simultaneously Negative Bulk Modulus and Mass Density," *Physical Review Letters*, 99(9):093904-1–093904-4.

Esteve, S. and Johnson, M. 2005. "Adaptive Helmholtz Resonators and Passive Vibration Absorbers for Cylinder Interior Noise Control," *Journal of Sound and Vibration*, 288:1105–1130.

Fang, N., Xi, D., Xu, J., Ambati, M., Srituravanich, W., Sun, C. and Zhang, X. 2006. "Ultrasonic Metamaterials with Negative Modulus," *Nature Materials*, 5:452–456.

Farhat, M., Enoch, S., Guenneau, S. and Movchan, A. 2008. "Broadband Cylindrical Acoustic Cloak for Linear Surface Waves in a Fluid," *Physical Review Letters*, 101(13):134501-1–134501-4.

Gil, M., Bonache, J. and Martín, F. 2008. "Metamaterial Filters: A Review," *Metamaterials*, 2:186–197.

Huang, L. 1999. "A Theoretical Study of Duct Noise Control by Flexible Panels," *Journal of the Acoustical Society of America*, 106(4):1801–1809.

Huang, L. 2002. "Modal Analysis of a Drum-like Silencer," *Journal of the Acoustical Society of America*, 112(5):2014–2025.

Huang, L., Choy, Y., So, R.M.C. and Chong, T. 2000. "Experimental Study of Sound Propagation in a Flexible Panel," *Journal of the Acoustical Society of America*, 108(2):624–631.

Huang, H., Sun, C. and Huang, G. 2009. "On the Negative Effective Mass Density in Acoustic Metamaterials," *International Journal of Engineering Science*, 47:610–617.

Izumi, T., Takami, H. and Narikiyo, T. 1991. "Muffler System Controlling an, Aperture Neck of a Resonator," *Journal of the Acoustical Society of Japan*, 47(9):647–652.

Jensen, L. and Chan, C.T. 2004. "Double-negative Acoustic Metamaterial," *Physical Review E*, 70(5):055602-1–055602-4.

Krokhin, A., Arriaga, J. and Gumen, L. 2003. "Speed of Sound in Periodic Elastic Composites," *Physical Review Letters*, 91(26):263402-1–263402-4.

Lapine, M. 2007. "The Age of Metamaterials," *Metamaterials*, 1:1.

Mei, J., Liu, Z., Wen, W. and Sheng, P. 2006. "Effective Mass Density of Fluid-solid Composites," *Physical Review Letters*, 96(2):024301-1–024301-4.

Merlin, R. 2004. "Analytical Solution of the Almost-perfect-lens Problem," *Applied Physics Letters*, 84(5):1290–1292.

Pendry, J.B. 2000. "Negative Refraction Makes a Perfect Lens," *Physical Review Letters*, 85(18):3966–3969.

Rossing, T.D. 2007. *Springer Handbook of Acoustics*, Springer, New York.

Shamonina, E. and Solymar, L. 2007. "Metamaterials: How the Subject Started," *Metamaterials*, 1:12–18.

Shena, J.T. and Platzman, P.M. 2002. "Near Field Imaging with Negative Dielectric Constant Lenses," *Applied Physics Letters*, 80(18):3286–3288.

Torrent, D., Hakansson, A., Cervera, F. and Sanchez-Dehesa, J. 2006. "Homogenization of Two-dimensional Clusters of Rigid Rods in Air," *Physical Review Letters*, 95(20):204302-1–204302-4.

Torrent, D. and Sanchez-Dehesa, J. 2007. "Acoustic Metamaterials for New Two-dimensional Sonic Devices," *New Journal of Physics*, 9:1–13.

Torrent, D. and Sanchez-Dehesa, J. 2008. "Anisotropic Mass Density by Two-dimensional Acoustic Metamaterials," *New Journal of Physics*, 10:1–25.

Torrent, D., Sanchez-Dehesa, J. and Cervera, F. 2007. "Evidence of Two-dimensional Magic Clusters in the Scattering of Sound," *Physical Review B*, 75(24):241404-1–241404-4.

von Flotow, A., Beard, A. and Bailey, D. 1994. "Adaptive Tuned Vibration Absorbers: Tuning Laws, Tracking, Agility, Sizing, and Physical Implementations," *Noise-Con 94*, Ft. Lauderdale, FL, pp. 437–454.